Supplementary Information

Figure S1. Related to Figure 1. The docking studies of A) 3-methyl transposed indole analog (later prepared as compound **4**) and B) 3-methyl-2-methylamino transposed indole analog (later prepared as compound **11**) to KasA using Autodock Vina (Vers. 1.1.2).
Figure S2. Related to Tables 1 and 2. Synthetic route to A) and B) transposed indoles and C) transposed indazoles.
Figure S3. Related to Tables 1 and 2. The kill kinetics of indoles A) **9** and B) **10**, and C) JSF-3285 at 10x MIC versus *M. tuberculosis* H37Rv and reduction of intracellular *M. tuberculosis* mc^26206 infection in J774.1 cells by indoles D) **9** and E) **10** and F) JSF-3285 with G) INH and H) RIF as controls.
Figure S4. Related to Figure 2. Unidentified electron density near the compound **9** binding site.
Figure S5. Related to Figure 2. Structural comparison of KasA-DG167 and KasA-**9**/**10**.
Figure S6. Related to Tables 1 and 2. Plot of plasma concentration (C_{plasma}) as a function of time for a single 25 mg/kg oral dose study in mice of A) compound 9, B) compound 10, C) DG167, D) compound 5g, E) compound 12 (JSF-3285), F) compound 13, G) compound 14, H) compound 15, and I) compound 16.
Figure S7. Related to Table 2. Analysis of compound modulation of *M. tuberculosis* mycolic acid biosynthesis by **JSF-3285**.

Table S1. Related to Table 1. *M. tuberculosis* MIC and Vero cell CC_{50} data for additional transposed indole analogs.
Table S2. Related to Tables 1 and 2. Activity of A) select transposed indoles (tabulated MIC values are in μM) versus clinical drug-resistant *M. tuberculosis* strains,(Vincent et al., 2012; Wilson et al., 2013), B) JSF-3285 versus select ESKAPE bacteria, and C) JSF-3285 versus clinical drug-resistant *M. tuberculosis* strains.
Table S3. Related to Tables 1 and 2. Activity of A) compounds **9** and **10** and JSF-3285 versus DG167-resistant *M. tuberculosis* mutants and B) JSF-3285 versus JSF-3285 spontaneous resistant *M. tuberculosis* mutants.
Table S4. Related to Figures 2 and 4. Data collection and refinement statistics for the X-ray crystal structures of KasA with bound compound **9**, compound **10**, or JSF-3285.
Table S5. **Related to Table 1.** Mouse pharmacokinetic profiling of select indole compounds.
Table S6. **Related to Tables 1 and 2.** A) Plasma protein binding (PPB) and plasma stability and B) cytochrome P450 inhibition for compounds **9**, **10**, and **JSF-3285**.
Table S7. Related to Tables 1 and 2. Dose escalation and tolerability data for compounds A) **9**, B) **10**, and C) JSF-3285.

Figure S1. Related to Figure 1. The docking studies of A) 3-methyl transposed indole analog (later prepared as compound **4**) and B) 3-methyl-2-methylamino transposed indole analog (later prepared as compound **11**) to KasA using Autodock Vina Vers. 1.1.2. Each ligand was prepared for docking experiment by adding hydrogens at pH 7.4 and minimizing the input geometry with the MMFF94 force field using Avogadro (Vers.1.2.0). The rotatable bonds were defined and Gasteiger partial charge was calculated in AutoDock Tools (Vers. 1.5.6). The hydrogen substituent at the C2 of the indole projected out of the pocket and the structure overlayed in green is $DG167_A$ in the same binding site. The predicted binding mode for this analog retains the key interactions of DG167 with the $DG167_A$ binding site, while having the 3-methyl moiety mimic interactions of the DG167 1-methyl with Pro201 and Pro206, places the *n*-butylsulfonamide into the hydrophobic channel formed by Ile202, Phe239, and Ile347, and maintains a hydrogen bond between the sulfonamide N-H and Glu-199. In addition, the indole-NH was predicted to be positioned to hydrogen bond with Glu203.

A)

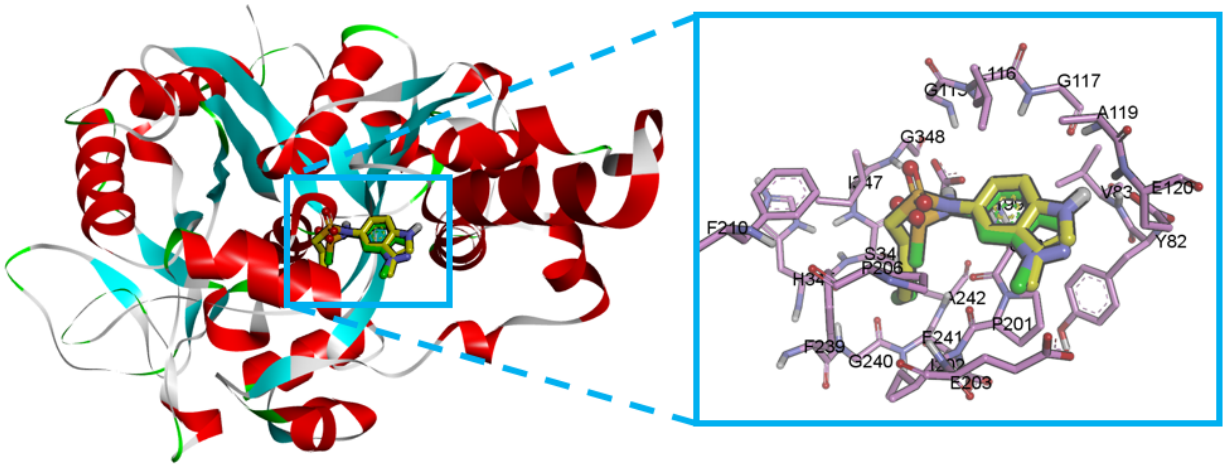

B)

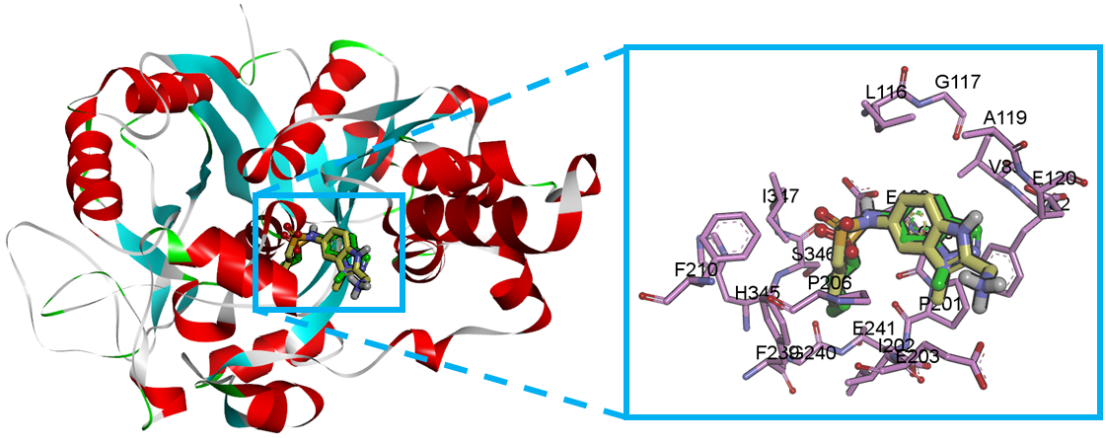

Figure S2. Related to Tables 1 and 2. Synthetic route to A) and B) transposed indoles and C) transposed indazoles. A) To access the 3-methyl-*1H*-indole analogs, we first synthesized the *N*-Boc-2'-bromo-5'-aminoacetophenone in two steps.(Bartoli et al., 2009) The *N*-Boc-protected ethyl 3-methyl-*1H*-indole-2-carboxylate **A1** was obtained by a ligand-free copper-catalyzed cascade reaction.(Cai et al., 2009) The 5-amino intermediate **A2** was provided upon TFA-mediated cleavage of the Boc group. The resulting amine **A2** was sulfonylated with *n*-butylsulfonyl chloride in presence of 2,6-lutidine to obtain *n*-butyl sulfonamide indole **5**. Saponification of the ethyl ester proceeded smoothly using LiOH in 1,4-dioxane with mild heating. The activation of acid **6** as a pentafluorophenyl (Pfp) ester **A3** and the subsequent treatment of the ester with aqueous ammonia provided the primary amide **8**. Direct routes from an ethyl ester to the parent amide reported in the literature(Csomós et al., 2007; Zhou et al., 2015) failed in our hands to provide **8** in satisfactory yield and reasonable reaction times. Initial attempts to reduce amide **8** with a variety of reducing agents (e.g., $LiAlH_4$, BH_3•THF) failed to provide the desired amine **11**.(Csomós et al., 2007; Csomós et al., 2006; Zhou et al., 2015) Several publications reported successful reductions of indole amides via the intermediate nitrile.(El-Fehail Ali et al., 1999; Steinman, 1978) Accordingly, we dehydrated the amide **8** with $POCl_3$ to provide nitrile **9**. While reductions of 2-nitrile indoles in the literature implemented $LiAlH_4$, we were only able to detect the imine intermediate as the major product. Instead, $NaBH_4$ in the presence of nickel(II) chloride was able to reduce the nitrile to the desired amine **11**.(Caddick et al., 2000; Khurana and Kukreja, 2002) B) The parent 3-methyl-*1H*-indole **4**, with a hydrogen 2-substituent, was synthesized by a Mizoroki-Heck reaction starting from commercially available 2-bromo-4-nitroaniline and allyl bromide.(Hennequin et al., 2003) C) Synthetic route to transposed indazoles. The nitro group in each starting indazole was reduced to the amine of type C1 via Pd-catalyzed hydrogenation or with tin(II) chloride in methanol with mild heating. The resulting 3-substituted 5-amino-*1H*-indazole was sulfonylated using the appropriate sulfonyl chloride in dry pyridine to afford the target compounds. (a) Pd/C, H_2, EtOH, (b) RSO_2Cl, pyridine, 0 °C to rt. (c) $SnCl_2$•$2H_2O$, EtOH, reflux (d) RSO_2Cl, pyridine, 0 °C to rt.

A)

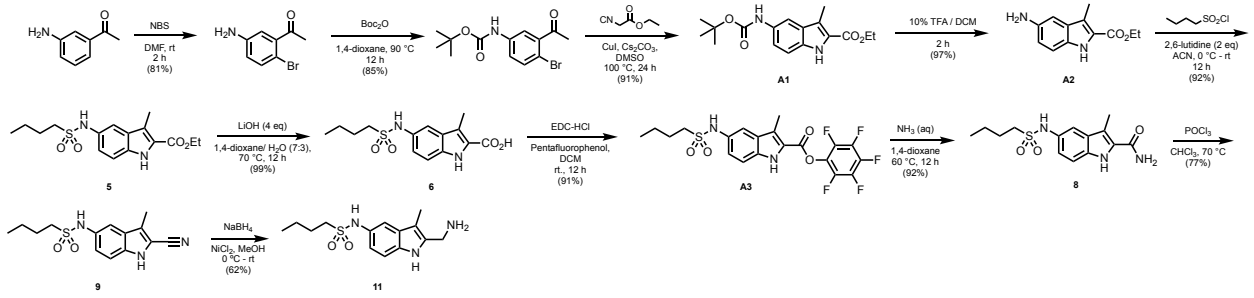

B)

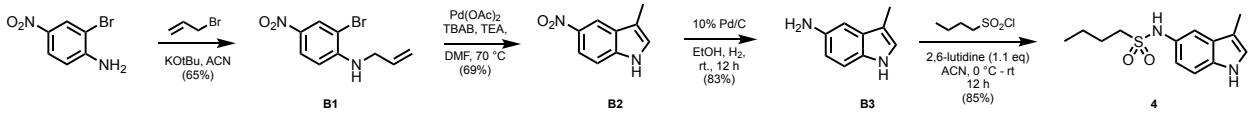

C)

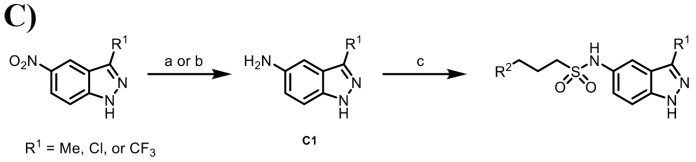

Figure S3. Related to Tables 1 and 2. The kill kinetics of indoles A) **9** and B) **10**, and C) JSF-3285 at 10x MIC versus *M. tuberculosis* H37Rv and reduction of intracellular *M. tuberculosis* mc^{2}6206 infection in J774.1 cells by indoles D) **9** and E) **10** and F) JSF-3285 with G) INH and H) RIF as controls. For kill kinetics, the comparisons include INH and DMSO in all cases, and in some cases, DG167 or the select analog with DG167 or INH (each also at 10x MIC). The samples were drawn from the same culture flasks (initial volume of 40 mL each) over the duration of the experiment and plated in three technical replicates to count CFUs. The *M. tuberculosis* infected cells were exposed to compounds at set concentrations for 72 h and the residual cell viability (%) was measured by luminescence assay. Each IC_{50} result was expressed as the mean ± standard deviation of triplicates from one of two independent experiments. All data were plotted using GraphPad Prism 8.1.2 with errors bars calculated from the standard deviation from three technical replicates.

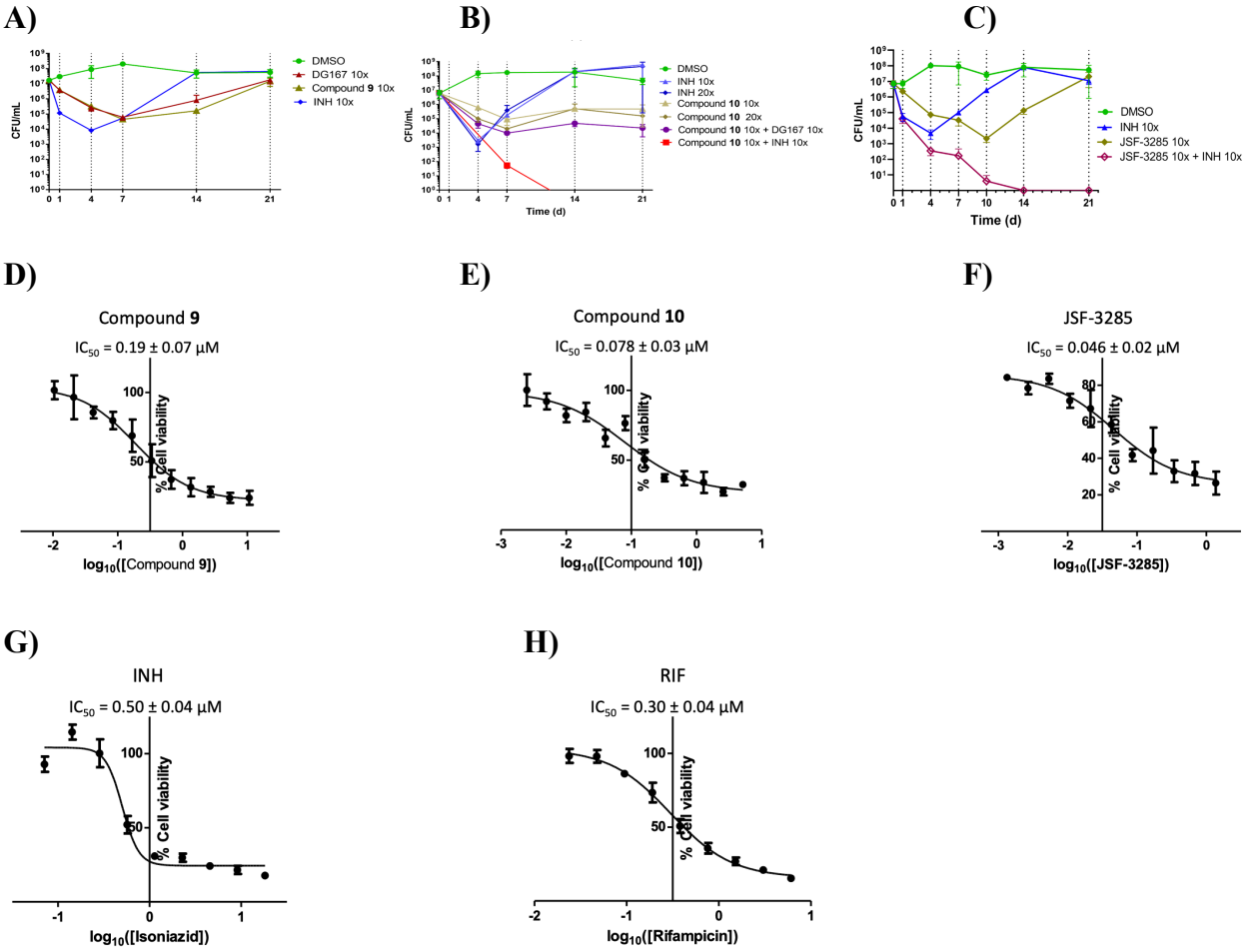

Figure S4. Related to Figure 2. Unidentified electron density near the compound 9 binding site. An image of the unidentified electron density found near compound **9** in the KasA substrate binding pocket. KasA residues and **9** are depicted as yellow sticks, water molecules are depicted as red asterisks, the blue mesh represents the $2F_o$-F_c map scaled to 1.0σ, and the green mesh represents the F_o-F_c map scaled to 3.0σ. Image generated in Coot.(Emsley et al., 2010)

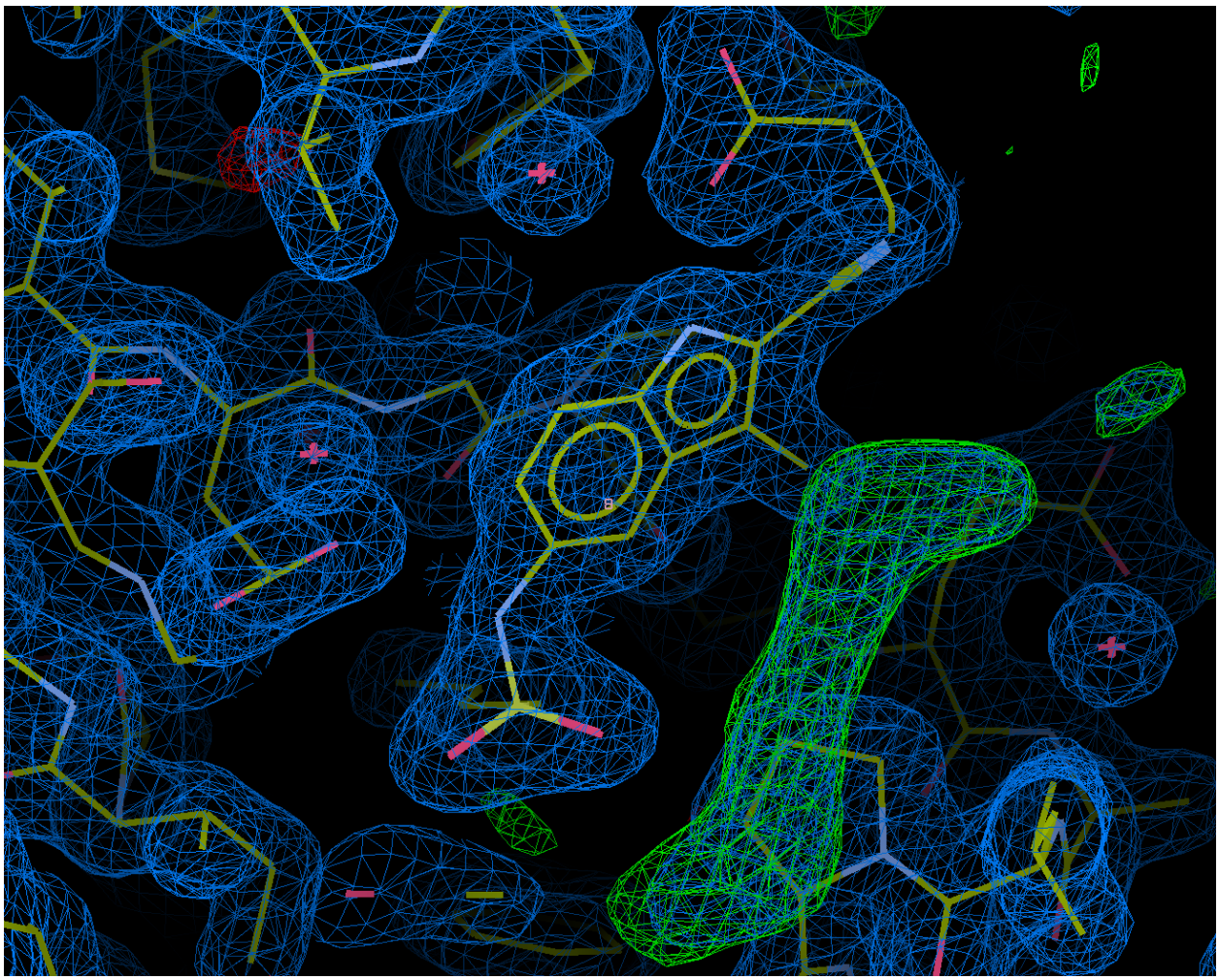

Figure S5. Related to Figure 2. Structural comparison of KasA-DG167 and KasA-9/10. A) Two molecules of DG167 ($DG167_A$ and $DG167_B$) bind to KasA (PDB ID 5W2P). B) Schematic representation of $DG167_A$ interactions. C) Compound **9** modeled into the $DG167_B$ binding site (a second copy of **9** or **10** for D) was modeled into the $DG167_B$ site with PyMol Version 1.8.2.3(Delano, 2002) using $DG167_B$ as a scaffold to which the requisite modifications were made) revealed a steric clash with the KasA surface highlighted by the dashed red box. D) Compound **10** modeled into the $DG167_B$ binding site revealed a steric clash with the KasA surface highlighted by the dashed red box. E) Structural alignment of KasA-**9** and KasA-**10** using the KasA Cα atoms. F) Isolated and rotated view of compounds **9** and **10** from the structural alignment depicted in E). Molecules are labeled consistently throughout the figure. KasA is depicted as either a cyan surface or sticks. $DG167_A$ is depicted as either green balls-and-sticks or bonds. $DG167_B$ is depicted as magenta bonds. 9_{clash} is depicted as yellow balls-and-sticks. 10_{clash} is depicted as pink balls-and-sticks. Hydrogen bonds are depicted as dashed lines measured in Å. The blue semicircles with radiating lines represent hydrophobic contacts mediated by KasA residues. The schematic was produced with LIGPLOT.(Wallace et al., 1995)

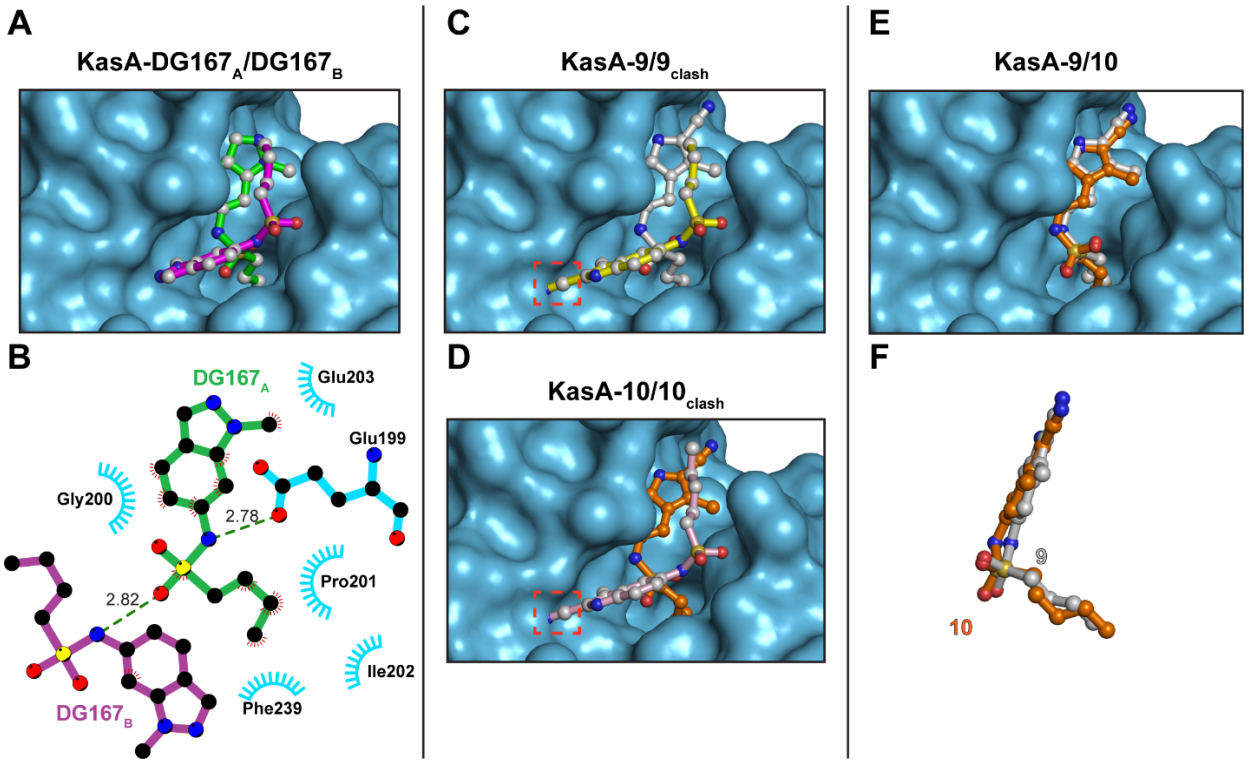

Figure S6. Related to Tables 1 and 2. Plot of plasma concentration (C_{plasma}) as a function of time for a single 25 mg/kg oral dose study in mice of A) compound **9**, B) compound **10**, C) DG167, D) compound **5g**, E) compound **12** (JSF-3285), F) compound **13**, G) compound **14**, H) compound **15**, and I) compound **16**. The red dotted line in each graph represents the MIC of each compound.

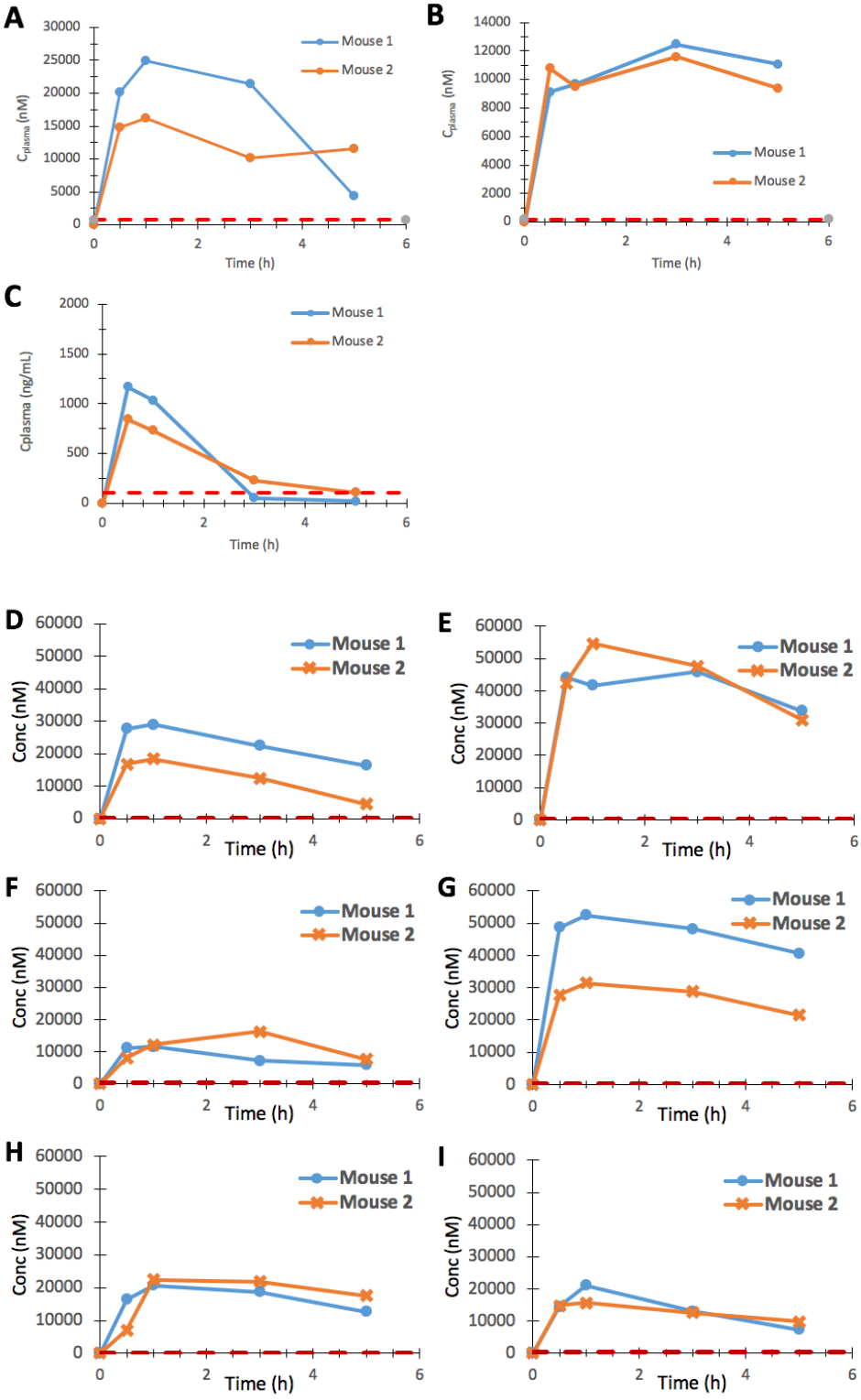

Figure S7. Related to Table 2. Effect of JSF-3285 on *M. tuberculosis* mycolic acid biosynthesis using ^{14}C-acetate labeling of newly synthesized fatty acids (FAMEs) and mycolic acids (MAMEs). A) Normal-phase TLC showing effect of JSF-3285 on *M. tuberculosis* H37Rv. B) Quantification of bands in panel A TLC and two additional replicates. C) Reverse-phase TLC analysis showing effects on FAMEs in select samples from panel A. D) Quantification of bands in panel C TLC and two additional replicates (mean values are depicted). E – H) Normal-phase TLC analysis of MAMEs from JSF-3285 resistant isolates of *M. tuberculosis*: E – strain 8x5 and G – strain 16x16 (Table S3B) with F and H depicting quantification of panels E and G with two additional replicates each, respectively. The TLCs were visualized by phosphorimaging, quantified using ImageQuant Total Lab, and plotted using GraphPad Prism 8.1.2.

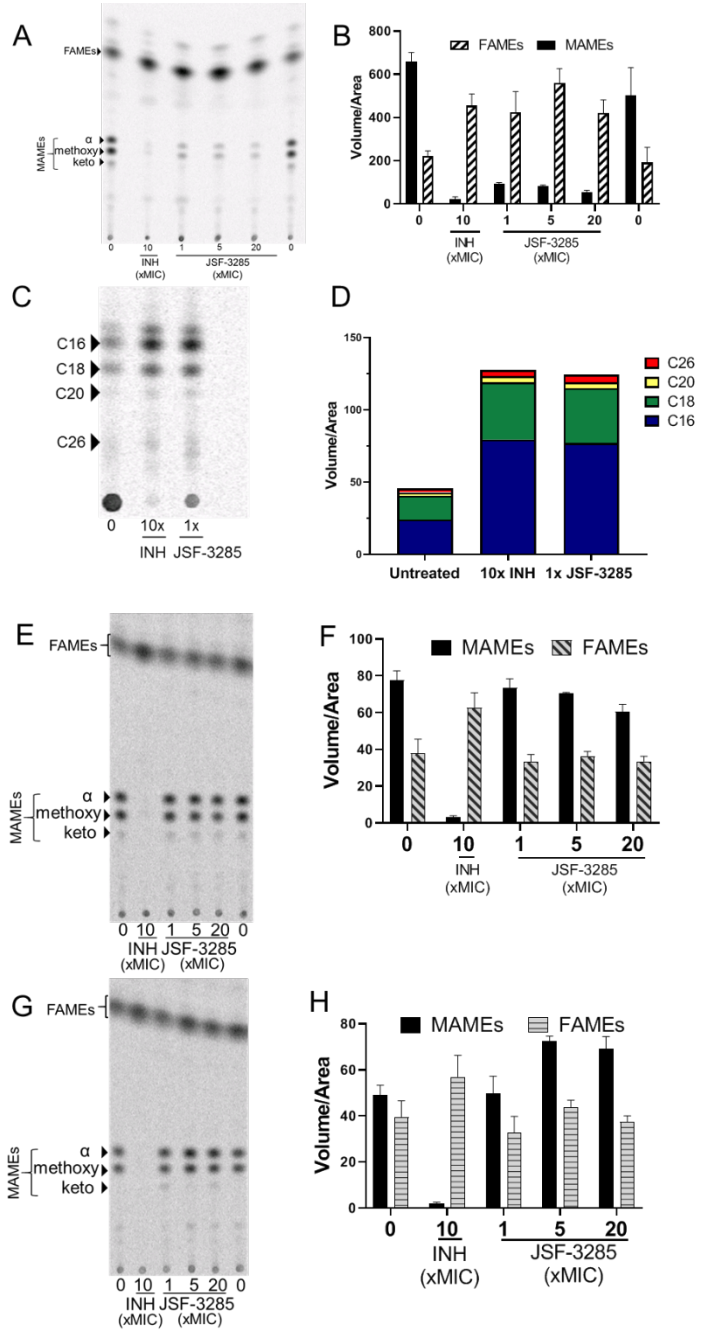

Table S1. Related to Table 1. *M. tuberculosis* MIC and Vero cell CC_{50} data for additional transposed indole analogs.

Cmpd	R^1	R^2	MIC H37Rv (μM)	Vero CC_{50} (μM)
1	CO_2Et	$NHCO_2$-*t*-Bu	>100	>160
2	CO_2Et	NH_2	>100	110
3	H	NO_2	>100	140
6	CO_2H	$NHSO_2$-*n*-Bu	>100	>160
7	CH_2OH	$NHSO_2$-*n*-Bu	>100	>170
12	CH_2NHAc	$NHSO_2$-*n*-Bu	>100	>150

Table S2. Related to Tables 1 and 2. Activity of A) select transposed indoles (tabulated MIC values are in μM) versus clinical drug-resistant *M. tuberculosis* strains,(Vincent et al., 2012; Wilson et al., 2013), B) JSF-3285 versus select ESKAPE bacteria, and C) JSF-3285 versus clinical drug-resistant *M. tuberculosis* strains.

A)

Cmpd	H37Rv	TDR31[a]	TDR91[b]	TDR116[c]
9	0.78	0.39	0.39	0.78
10	0.20	0.20	0.10	0.20
INH	0.40	>12	>12	>12

[a]Resistant to INH, RIF, ethambutol, kanamycin, streptomycin, and capreomycin
[b]Resistant to INH, RIF, and ethambutol
[c]Resistant to INH, ethambutol, *p*-aminosalicylic acid

B)

Organism	Strain	JSF-3285 MIC (μM)
A. baumannii	ATCC 19606	>50
E. cloacae	ATCC 13047	>50
E. faecium	NCTC 7171	>50
K. pneumoniae	BAA 2146	>50
P. aeruginosa	HER 1018	>50
S. aureus	ATCC 43300	>50

C)

Strain	Geographic Isolation	Resistance profile	JSF-3285 MIC (μM)
H37Rv	Laboratory strain	Pan-susceptible	0.39
TDR29	Azerbaijan	Pan-susceptible	0.195
TDR1	Bangladesh	Pan-susceptible	0.195
TDR126	Brazil	Pan-susceptible	0.39
TDR138	Germany	Pan-susceptible	0.195
TDR173	Philippines	Pan-susceptible	0.39
TDR91	South Korea	Pan-susceptible	0.0975
TDR128	Brazil	EMB	0.195
TDR156	Peru	EMB	0.39
TDR92	South Korea	EMB	0.39

TDR143	Germany	SM	0.0975
TDR146	Nepal	SM	0.195
TDR74	Rwanda	INH, RIF	0.39
TDR150	Rwanda	INH, RIF	0.39
TDR106	South Korea	INH, RIF	0.0975
TDR42	Bangladesh	INH, EMB	0.195
TDR132	Brazil	INH, EMB	0.78
TDR195	Morocco	INH, EMB	0.39
TDR104	South Korea	INH, EMB	0.195
TDR109	South Korea	INH, SM	0.39
TDR73	Peru	INH, RIF, EMB	0.0975
TDR21	RD Congo	INH, RIF, EMB	0.195
TDR101	Rwanda	INH, RIF, EMB	0.78
TDR114	Rwanda	INH, RIF, EMB	0.0975
TDR162	Rwanda	INH, RIF, EMB	0.0975
TDR99	South Korea	INH, RIF, EMB	0.0975
TDR26	Abkhazia	INH, RIF, SM	0.195
TDR6	Bangladesh	INH, RIF, SM	0.195
TDR36	Bangladesh	INH, RIF, SM	0.0975
TDR37	Bangladesh	INH, EMB, SM	0.0975
TDR93	South Korea	INH, EMB, SM	0.195
TDR105	South Korea	INH, EMB, SM	0.39
TDR120	South Korea	INH, EMB, SM	0.195
TDR123	South Korea	INH, EMB, SM	0.39
TDR19	Azerbaijan	INH, RIF, EMB, SM	0.195
TDR7	Bangladesh	INH, RIF, EMB, SM	0.195
TDR32	Bangladesh	INH, RIF, EMB, SM	<0.0975
TDR133	Brazil	INH, RIF, EMB, SM	0.0975
TDR50	Burundi	INH, RIF, EMB, SM	0.195
TDR58	Burundi	INH, RIF, EMB, SM	0.195
TDR192	Guinea	INH, RIF, EMB, SM	0.195
TDR196	India	INH, RIF, EMB, SM	0.0975
TDR31	Kazakhstan	INH, RIF, EMB, SM	0.195
TDR191	Peru	INH, RIF, EMB, SM	0.195
TDR216	Peru	INH, RIF, EMB, SM	0.195
TDR67	Rwanda	INH, RIF, EMB, SM	0.0975
TDR72	Rwanda	INH, RIF, EMB, SM	0.0975
TDR87	South Korea	INH, RIF, EMB, SM	0.195
TDR116	South Korea	INH, RIF, EMB, SM	0.0975
TDR124	South Korea	INH, RIF, EMB, SM	0.78

Table S3. Related to Tables 1 and 2. Activity of A) compounds **9** and **10** and JSF-3285 versus DG167-resistant *M. tuberculosis* mutants and B) JSF-3285 versus JSF-3285 spontaneous resistant *M. tuberculosis* mutants. Tabulated MIC values are in μM.

A)

Cmpd	H37Rv	DRM167 16x3	DRM167 8x3	DRM167 16x6	DRM167 8x2	DRM167 32x11	DRM167 32x2
	WT	V123A	I145T	I122S	A119T	G240S	P206T
DG167	0.39	1.6	6.2	50	50	100	>100
9	0.78	100	>100	>100	>100	>100	>100
10	0.20	>100	>100	>100	>100	>100	>100
JSF-3285	0.39	25	>100	>100	>100	>100	>100
INH	0.19	0.19	0.19	0.19	0.19	0.19	0.19

B)

Strain	*kasA*-SNP[a]	KasA[b]	MIC (μM)		
			DG 167	JSF-3825	INH
H37Rv	none	none	0.39	0.39	0.31
DRM 3285 4x1	gAa-gCa	E199A	>100	>100	0.63
DRM 3285 4x2	gAa-gCa	E199A	>100	>100	0.31
DRM 3285 8x3	Atg-Gtg	M277V	>100	>100	0.16
DRM 3285 8x4	cCc-cTc	P147L	100	50	1.25
DRM 3285 8x5	gGa-gCa	G200A	>100	>100	0.16
DRM 3285 8x6	cCc-cTc	P147L	>100	100	0.31
DRM 3285 8x7	cCc-cTc	P147L	>100	50	0.31
DRM 3285 8x8	cCc-cTc	P147L	50	12.5	0.31
DRM 3285 16x9	gTg-gCg	V137A	>100	>100	0.16
DRM 3285 16x10	Atg-Gtg	M277V	nd	nd	nd
DRM 3285 16x11	cCc-cTc	P147L	100	100	0.31
DRM 3285 16x12	Gtt-Ctt	V142L	100	100	0.31
DRM 3285 16x13	aTc-aAc	I145N	>100	>100	nd
DRM 3285 16x14	Atg-Gtg	M277V	>100	>100	0.31
DRM 3285 16x15	Atg-Gtg	M277V	>100	>100	0.31
DRM 3285 16x16	cTg-cCg	L205P	>100	>100	0.31

[a] Capitalized letter in the codon shows nucleotide change

[b] Row indicates amino acid substitution corresponding to *kasA*-SNPs

nd = Not Determined

Table S4. Related to Figures 2 and 4. Data collection and refinement statistics for the X-ray crystal structures of KasA with bound A) compound **9**, compound **10**, or JSF-3285.

	KasA-**9**	KasA-JSF3285	KasA-**10**
PDB ID	6P9K	6P9L	6P9M
Data collection			
Space group	$P3_121$	$P3_121$	$P3_121$
Cell dimensions			
a, b, c (Å)	77.51, 77.51, 145.17	77.80, 77.80, 146.37	77.71, 77.71, 146.44
α, β, γ (°)	90.0, 90.0, 120.0	90.0, 90.0, 120.0	90.0, 90.0, 120.0
Resolution (Å)	50.00-1.70 (1.75-1.70)	50.00-2.30 (2.34-2.30)	50.00-2.25 (2.29-2.25)
Wavelength (Å)	0.88557	0.97946	0.97946
Completeness (%)	99.9 (100.0)	99.7 (97.1)	99.0 (97.0)
R_{sym} (%)	6.4 (54.6)	8.8 (57.1)	4.8 (69.8)
$CC^{1/2}$	0.999 (0.932)	0.997 (0.928)	0.999 (0.953)
Average I / σI	41.2 (3.2)	46.8 (4.6)	38.1 (2.4)
Redundancy	9.9	9.5	9.9
Total reflections	553,090	219,910	243,851
Unique reflections	55,980	23,255	24,547
Refinement			
R_{work} / R_{free} (%)	14.43 (16.41) / 16.93 (19.92)	17.12 (22.69) / 20.43 (29.35)	19.68 (39.57) / 23.15 (41.79)
Number of atoms			
All atoms	3419	3165	3189
Protein	3085	3042	3042
Ligand	20	19	21
Glycerol	6	6	12
2-propanol	20	20	12
Ions	1	1	1
Water	287	77	101
Average B-factor ($Å^2$)			
All atoms	35.57	63.17	67.54
Protein	34.66	63.19	67.78
Ligands	45.34	42.40	74.12
Water	43.77	56.68	57.38
R.m.s. deviations			
Bond lengths (Å)	0.009	0.003	0.002
Bond angles (°)	1.018	0.555	0.480
Ramachandran statistics			
Favored (%)	97.33	96.84	97.09
Allowed (%)	2.43	2.92	2.57
Outliers (%)	0.24	0.24	0.24

Data collection and refinement statistics. $R_{sym} = \Sigma_h \Sigma_i | I_i(h) - \langle I(h) \rangle | / \Sigma_h \Sigma_i I_i(h)$, where $I_i(h)$ is the i^{th} measurement of h and $\langle I(h) \rangle$ is the mean of all measurements of I(h) for reflection h. $R_{work} = \Sigma ||F_o| - |F_c|| / \Sigma |F_o|$, calculated with a working set of reflections. R_{free} is R_{work} calculated with only the test set of reflections. Data for the highest resolution shell are given in parentheses. The structures were determined using single crystals.

Table S5. **Related to Table 1.** Mouse PK profiling of select indole compounds.

	Compound 9	**Compound 10**	**DG167**
Plasma $AUC_{0\text{-}5h}$ [a] (h*ng/mL)	21511	15624	1965
C_{max} [a] (ng/mL)	7260	3800	1030
MIC (ng/mL)	230	61	100
Plasma $AUC_{0\text{-}5h}$ /MIC [a]	93	260	20
C_{max}/MIC [a]	31	62	10
T>MIC [a] (h)	≥5	≥5	3 – 5
C_{lung}/C_{plasma} at 5 h	2.54	0.96	nd
$t_{1/2}$ [b] (h)	1.03	1.30	0.54
Clearance [b] (mL/h*kg)	980.9	682.4	2855.1
V_d (L/kg) [b]	1.45	1.28	2.21

[a] Average of two mice following administration of a single 25 mg/kg po dose
[b] Average of three mice following administration of a single 5 mg/kg iv dose
nd = not determined

Table S6. **Related to Tables 1 and 2.** A) Plasma protein binding (PPB) and plasma stability and B) cytochrome P450 inhibition for compounds **9**, **10**, and **JSF-3285**.

A)

Cmpd	Human PPB (%)	Human plasma Stability @ 5 h (%)	Mouse PPB (%)	Mouse plasma Stability @ 5 h (%)
9	97.4	93.5	96.1	95.5
10	99.4	>99.9	98.0	87.0
JSF-3285	77.4	83.0	62.8	>99.9

B)

Cmpd	Cytochrome P450 1A2 Inhibition IC_{50} (μM)	Cytochrome P450 2C9 Inhibition IC_{50} (μM)	Cytochrome P450 2C19 Inhibition IC_{50} (μM)	Cytochrome P450 2D6 Inhibition IC_{50} (μM)	Cytochrome P450 3A4 Inhibition IC_{50} (μM)
9	4.90	5.08	1.72	3.56	7.46
10	5.00	1.94	0.542	1.47	1.47
JSF-3285	>50	>50	>50	>50	>50

Table S7. Related to Tables 1 and 2. Dose escalation and tolerability data for compounds A) **9,** B) **10**, and C) JSF-3285.

A)

Dose (mg/kg)	Average $AUC_{0\text{-}24h}$ (h*ng/mL)	Dose corrected $AUC_{0\text{-}24h}$ ($AUC_{0\text{-}24h}$ /Dose)	Theoretical Proportionality	Dose Proportionality
25 [a]	14494.5	579.8	1.0	1.00
50	54977.1	1099.5	2.0	3.79
100	99454.2	994.5	4.0	6.86
250	335441.7	1341.8	10.0	23.14
500	395749.2	791.5	20.0	27.30

[a] 25 mg/kg data from 8-h PK study

B)

Dose (mg/kg)	Average $AUC_{0\text{-}24h}$ (h*ng/mL)	Dose corrected $AUC_{0\text{-}24h}$ ($AUC_{0\text{-}24h}$ /Dose)	Theoretical Proportionality	Dose Proportionality
25 [a]	16739.3	669.6	1.0	1.0
50	59569.9	1191.4	2.0	3.6
100	109779.8	1097.8	4.0	6.6
250	305004.3	1220.0	10.0	18.2
500	486227.0	972.5	20.0	29.0

[a] 25 mg/kg data from 8-h PK study

C)

Dose (mg/kg)	Average $AUC_{0\text{-}24h}$ (h*ng/mL)	Dose corrected $AUC_{0\text{-}24h}$ ($AUC_{0\text{-}24h}$ /Dose)	Theoretical Proportionality	Dose Proportionality
25 [a]	89415	3577	1	1.00
50	161453	3229	2	1.81
150	463752	3092	6	5.19
300	921700	3072	12	10.31

[a] 25 mg/kg data from 8-h PK study